IUST
Iran University of Science and Technology

Iranian Journal of Electrical and Electronic Engineering

Journal Homepage: ijeee.iust.ac.ir

Surrogate-Based Multiphysics Design Optimization of a Wound Rotor Synchronous Generator with Enhanced Damping

Ali Amini *, Farshid Mahmouditabar **(C.A.), Nick J. Baker **, and Abolfazl Vahedi*

Abstract: In recent years, due to the increase in electricity generation, the need for optimized Wound Rotor Synchronous Generators (WRSGs) has been felt more than ever. One of the important characteristics of a generator in a power system is its voltage harmonics. In addition to this, the amount of generated power and efficiency are also important. The goal of this research is multi-objective design using dampers, with improved number and shape. WRSGs have been selected as a case study. With the help of surrogate modeling and the PSO algorithm, which are more efficient and accurate than classical methods, the final design has been presented. In the end, the comparison of the initial and final designs shows the realization of all goals. Also, economic issues in terms of the selection of damper material have been investigated.

Keywords: wound rotor synchronous generator (WRSG), multi-objective optimization, surrogate modeling, damper design, total harmonic distortion (THD).

1 Introduction

WOUND Rotor Synchronous Generators (WRSGs) have rotor windings that offer distinct advantages, such as external control of rotor current through slip rings. Although, at first glance, this advantage may not seem significant due to its simplicity and general applicability, propelling WRSGs to the forefront of candidates for electricity generation, especially due to their ability to work over a wide range of angular velocities and generate voltage at the grid frequency [1]. In recent decades, the increasing demand for electrical energy [2], [3] has urged the engineering community to seek other types of generators alongside WRSGs, such as Permanent Magnet generators (PMGs) and Induction Generators (IGs), especially for low angular velocities [4] like those in wind turbines. Each of these three types has its own set of advantages and disadvantages, which are detailed in Table I [5], [6].

Harmonics that are not desired have significant negative effects on electricity systems; particularly in the context of WRSGs, they manifest as mechanical and electrical damages. Mechanically, harmonics periodically stress the generator shaft, which can lead to wear and a shortened lifetime for the generator over the long term. Electrically, harmonics distort the stator and rotor voltages, bringing about extra heating and losses, ultimately resulting in lower efficiency and functionality [7], [8]. In this regard, global standards have been set, and scholars are working to meet them by proposing effective harmonic mitigation methods [9], [10].

The ideal condition is when the generator's emf behaves purely sinusoidally; this is the final target of corrective measures such as distributed and short-slot windings [10]. However, what makes these measures somewhat disadvantageous is the complexity and cost they add to the generator, while also lowering the emf voltage. Damper cages within salient pole synchronous; these not only mitigate harmonics but also hinder transient voltage surges in unsteady loads. However, regular damper cages tend to higher rotor winding current, which is synonymous to higher losses [11]. To

Iranian Journal of Electrical & Electronic Engineering, 2026.
Paper first received 24 Apr 2026 and accepted 17 Sep 2026.
* The author is with the school of electrical engineering, Iran University of Science and Technology Tehran, Iran
** The authors are with the School of Engineering, Newcastle University, Newcastle Upon Tyne, UK.
Corresponding Author: Farshid Mahmouditabar
farshid.mahmouditabar@ncl.ac.uk

address this challenge, different configurations have been suggested, such as radial and tangential, which simultaneously lessen the Total Harmonic Distortion (THD) of SG voltage and losses [12].

What is significant but has been neglected in other investigations until now is the wide effect of the damper cage on generator behavior; since all of them were under no-load conditions, which do not fully reflect the generator's dynamics. Therefore, there is always a concern about the generator's degradation functionally, which leads engineers to minimize harmonics rather than completely remove them, keeping the THD of no-load line-to-line voltage in the range of 2 to 3% [13].

There is a lack of a design that can mitigate distortions with the least negative effect on generator operating conditions, and this study will try to address that as best as we can. Until now, a significant number of designs have been suggested in iterative form; each of them suffers from either a limited design set or long analysis times. Surrogate modeling could strike a balance in this regard and handle different objectives and limitations that were previously not gathered. In addition to model selection, method and algorithm selection are also central to this work, as they significantly affect the results of an iterative design. In the following study, we will first outline the design data for the WRSG; then, we will investigate load conditions, design goals, the chosen algorithm, sensitivity analysis, and the effect of materials to find the best available design. Finally, the first and final designs will be weighed against each other electrically.

Table 1. Comparison of Different Generator Topologies

Generator Type	Advantages	Disadvantages
Synchronous Generator	• Maximum speed range • Gearless Operation • Precise Control of Reactive and Active Power • Low THD • High efficiency	• An AC-DC-AC power conversion system is essential • A multipole configuration is preferred for direct-drive generators • Medium power density • High cost
Induction Generator	• Brushless • High power density • Maximum speed range • Medium cost	• Gearboxes are an essential component • Power conversion system is indispensable • Cannot control power factor • Medium efficiency
Permanent Magnet Synchronous Generator	• Gearless Operation • High power density • Low THD • High efficiency	• Permanent magnets are essential • An AC-DC-AC power conversion system is essential • Risk of demagnetization • High cost for rare earth PMs

2 Case Study Design

Design of a WRSG is a set of different concerns that should be considered, ranging from magnetic field generation to terminal voltage. The responsibility for magnetic field generation lies with the rotor field windings, which are fed with DC excitation. This leads to a rotary magnetic field that interacts with the armature windings to generate AC voltage. In this regard, the voltage of a WRSG can be written as below:

$$E = 4.44 \times f \times N \times \phi \quad (1)$$

where f, N, and ϕ are frequency (Hz), the number of stator winding turns, and magnetic flux (Wb), respectively. In other words, the calculation of stator winding turns in relation to the voltage is core to WRSG design. Moreover, providing a uniform magnetic flux distribution to minimize voltage harmonics has a dependency on the stator winding configuration as well as the rotor configuration. Optimizing the airgap flux distribution and taking advantage of multi-layer windings offer us benefits in line with THD minimization. If the airgap between the rotor and stator is chosen to be large, it is synonymous with higher magnetic losses and lower efficiency. On the other hand, a small airgap increases the risk of an early downturn. Large magnetic flux density means higher magnetic losses and a higher risk of magnetic saturation. In this regard, the design data for the investigated generator is shown in Table 2, while Fig. 1 shows its geometry, flux lines, and flux density. To account for the generator's dynamics in the redesign, it has been investigated under full-load conditions with a triangular load of 90 ohms, as shown in Fig. 2. To determine the optimal damper cage configuration that minimizes Total Harmonic Distortion (THD) while maintaining the generator's performance near its design targets, a one-at-a-time sensitivity analysis was performed. As illustrated in Fig. 3, different numbers of damper bars were evaluated to assess their impact on THD and output power. A trade-off was made between achieving low THD and preserving the desired power output. Based on this analysis and practical prototype constraints, the final selection was made, and

8 damper bars were identified as the most suitable configuration.

Table 2. Technical data of the investigated WRSG.

Designed Parameters	Unit	Value
Number of Phases	-	3
Number of Rotor Poles	-	6
Number of stator Slots	-	72
Rated Speed	RPM	1000
Dc Current	A	90
Winding Layers	-	2
Pole Tip Depth	mm	40
Stator Outer Diameter	mm	750
Stator Inner Diameter	mm	530
Slot Fill (field)	%	74
Slot Fill (Armature)	%	30
Stator Stack Length	mm	548
Lamination	-	M350-50A
Pole Depth	mm	100

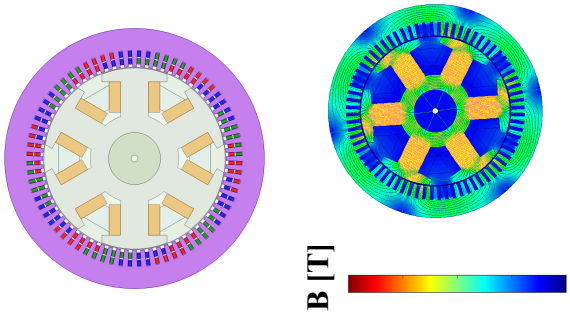

(a) (b)

Fig 1. The initial design of the investgated generator (a) geometry, and (b) flux lines, and flux density.

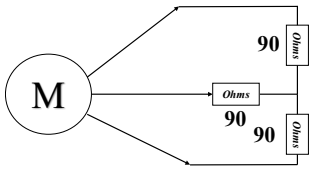

Fig 2. Three-phase star resistive load of 90 ohms.

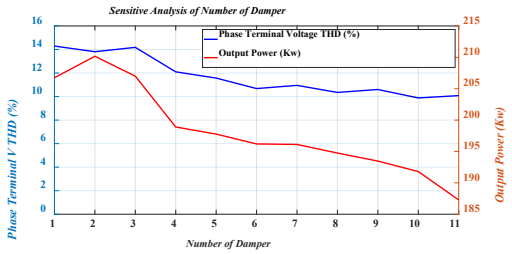

Fig 3. One-at-a-time sensitivity analysis of number of dampers.

3 Multi-Objective Optimization Algorithm

Our goal is a multi-objective redesign, leveraging surrogate modeling and the PSO algorithm due to its proficiency and collective intelligence in global search [14]. In this regard, our primary objectives are output power, efficiency, and phase terminal voltage THD. Our desires include improved output voltage profile, stabilized efficiency, and prevention of drastic output power drop resulting from corrective measures for voltage THD minimization. The detailed steps of the proposed multi-objective redesign are as follows, as shown in Fig. 4.

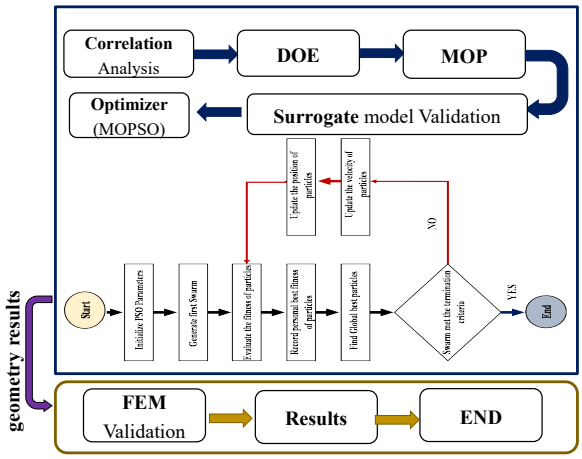

Fig 4. The detailed steps of the proposed multi-objective redesign.

3.1 Correlation Analysis and Design of Experiment (DOE)

The accuracy of correlation analysis is highly dependent on the number of designs. Therefore, Latin Hypercube Sampling (LHS) is the preferred sampling method due to its merits [15]. This sampling method ensures that the selected samples cover a broad design space, leading to more accurate optimization. After generating a satisfactory Design of Experiments (DOE) with 960 designs, the correlation, which measures the linear relationship between two variables with values between -1 and 1 [16], was extracted using the DOE and the results of the Finite Element Analysis (FEA). This is shown among the six variables in Fig. 5 and Table 3.

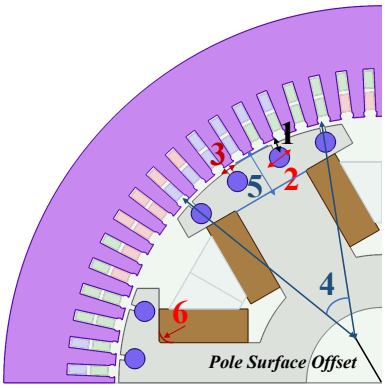

Fig 5. Six design variables: four are related to the damper, while the other two variables are related to the shape of the pole tip.

Table 3. Variables of the geometry optimization.

Optimization Variables	No.	Unit	Min	Max	Optimum Value
Damper Bar Depth	1	mm	0.1	2.5	2.46
Damper Bar Diameter	2	mm	2	10	9.55
Damper Bar Opening	3	mm	0.1	2.5	1.82
Damper Bar Pitch	4	Edeg	140	210	174.64
Pole Tip Depth	5	mm	30	45	30.06
Pole Tip Radius	6	mm	0	20	11.7

Of these six variables, four are related to the damper geometry to find the optimal form, while the other two variables are related to the shape of the pole tip. As depicted in Fig. 6, most of these variables have a significant effect on the generator's operating condition and are complementary to each other.

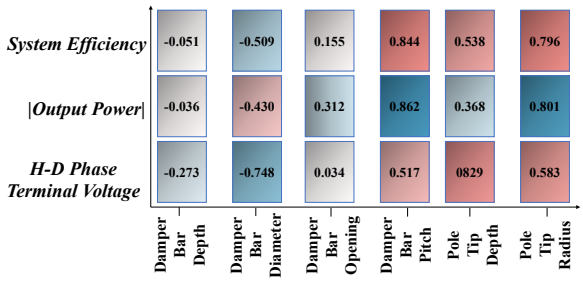

Fig 6. Correlation Analysis between generator optimization objects and design variables.

3.2 Surrogate Model

Given the complexity of the WRSG design problem—characterized by a high number of design variables and multiple conflicting objective functions, performing direct optimization using computationally expensive FEA for every design iteration becomes impractical [17]. To overcome this challenge and reduce computational costs, a surrogate modeling approach is adopted. This method establishes an approximate mathematical relationship between design variables and objective functions, enabling rapid prediction of system performance without resorting to full-scale simulations.

To construct the surrogate model, an optimized DOE obtained from the earlier stage is used. Among the available techniques, Anisotropic Kriging is selected due to its superior accuracy compared to standard Kriging and Response Surface Methodology (RSM), while maintaining lower complexity than Artificial Neural Networks (ANN) [18]. Anisotropic Kriging is particularly effective in cases where the response is influenced differently along various input directions. Unlike classical Kriging, which assumes an isotropic variogram, treating all directions equally, anisotropic Kriging allows the variogram to vary by direction, capturing directional trends in the data more accurately. This modelling approach introduces a unique variogram for each direction by considering both the magnitude and orientation of variable influences. As a result, it better captures the complex, multi-dimensional behavior present in WRSG performance metrics. The covariance structure between any two data points in the input space is central to Kriging-based models and is mathematically expressed by Eq. 2, which defines the correlation based on the spatial distance and direction between points. By leveraging anisotropic Kriging, the surrogate model in this study efficiently supports the multi-objective optimization process, enabling accurate performance prediction with reduced reliance on high-fidelity simulations. Theoretical details and derivations of both classical and anisotropic Kriging can be found in [4], and this work further builds on those foundations for application in electrical machine design.

$$\mathrm{Cov}(\bar{x}', \bar{x}'') := \sigma - \gamma(\bar{x}' - \bar{x}'') \tag{2}$$

In classical Kriging, only the magnitude of $(\bar{x}' - \bar{x}'')$ is considered. The anisotropic approach begins by estimating empirical directional variograms. To determine the i-th directional variogram, all point pairs (x_1, x_2) are collected from the dataset such that the vector $(x_2 - x_1)$ lies approximately parallel to the i-th coordinate axis. This condition is enforced by the following constraints.

$$(x_2 - x_1)^j < \lambda(x_2 - x_1)^i \quad \text{(e.g., } \lambda^{-1} = 2 \times \text{number of input variables)}, \qquad (x_2 - x_1)^j < M \tag{3}$$

where M is a tolerance threshold ($M = \frac{\max Lag - minLag}{10}$). After identifying these directional classes, an experimental directional variogram is constructed in the same way as in ordinary Kriging, without subclass grouping. The entire set of directional variograms is then fitted using the Levenberg–Marquardt procedure. For computational simplicity, a single variogram model is ultimately adopted across all directions, albeit with distinct ranges for each. In simpler terms, anisotropic Kriging models the variogram as a function of both distance and direction. This approach enhances both the accuracy and flexibility of the model using directional variograms and accommodates a broader range of variogram behaviors. However, this improvement comes at the cost of increased model complexity due to the necessity of analyzing directional dependencies.

In the modeling process, 20% of the data is used for validation, and 80% is used for training the model. The accuracy of the created model is of utmost importance; hence, it is necessary to validate it. For this purpose, two

parameters, MNE and R^2, are used. The meaning of these parameters is as Eqs. 4 and 5.

$$MNE = \frac{1}{m}\sum_{i=1}^{m}|\varepsilon_i|/(y_{\max} - y_{\min}) \quad (4)$$

$$R^2 = 1 - \sum_{i=1}^{m}\varepsilon_i^2 / \sum_{i=1}^{m}(y_i - M)^2 \quad (5)$$

The closer MNE is to zero and R^2 is closer to one, the higher the accuracy. Table 4 shows the evaluation of the surrogate models, and Fig. 7 shows the RSM distance for three functions, indicating that the data related to the surrogate model matches the FEA data with good accuracy during the model evaluation phase. Higher accuracy implies a greater similarity between the results of the optimization algorithm and FEA.

Table 4. Accuracy assessment of the trained Surrogate Models.

Objective and Constraint	MNE	R^2
System Efficiency	1.43e-2	0.993
Output Power	1.21e-2	0.993
THD Phase Terminal Voltage	4.53e-2	1

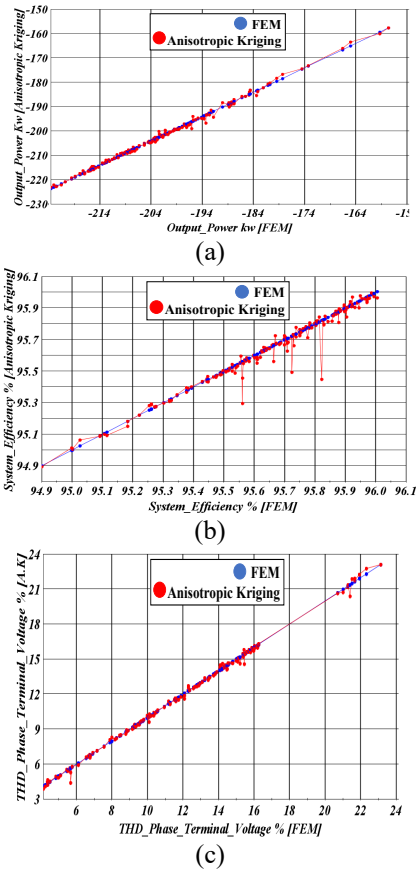

Fig 7. The RSM distance for three functions, indicating that the data related to the surrogate model matches the FEA data with good accuracy during the model evaluation phase.

3.3 PSO Algorithm

In this design, a maximum of 3000 designs and generations were considered. After generating 3000 designs, 89 were found to be unfeasible. Among the feasible designs, 321 were identified as part of the Pareto front. This demonstrates the high capability of the algorithm and justifies its use. In the next step, after the algorithm generates 321 Pareto fronts, to increase the accuracy in selecting the optimal design, the multi-objective optimization problem is transformed into a single-objective optimization problem using Eq. 6.

As shown in Eq. 6, the coefficients c_1, c_2, and c_3 are the weight coefficients of the optimization function, which are determined based on the importance of the function. In this optimization, due to the higher importance of the voltage harmonics function, it has higher weight coefficients. The goal is to find the minimum point of the function F. Ultimately, the optimal design is identified using this method. Design number 257, among the 321 designs, is the optimal design, and the values of the variables obtained from the optimization algorithm are presented in Table III. Additionally, Fig. 8 shows the plot of the function F, which clearly demonstrates the optimality of the found design.

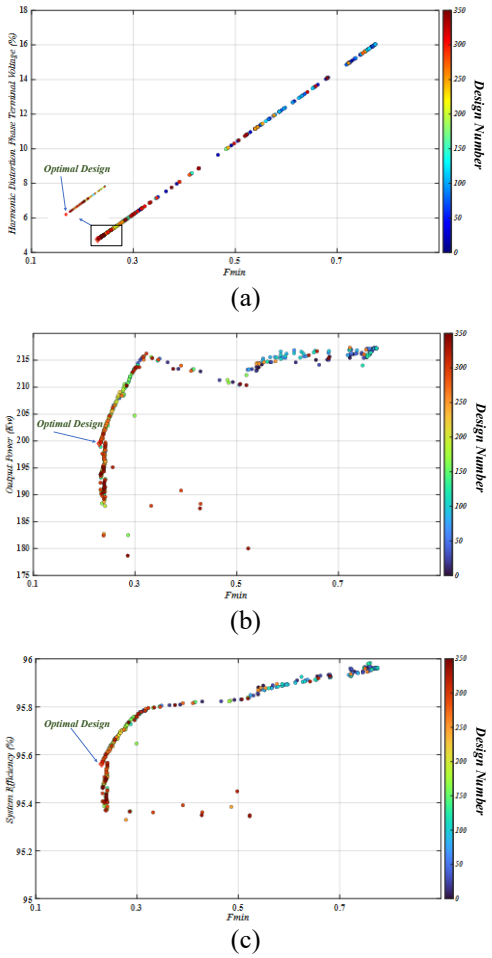

Fig 8. The plot of the function F, which clearly demonstrates the optimality of the found design.

$$F_{min} = c_1 \times \frac{Intial\ Output\ Power}{Output\ Power} + c_2 \times \frac{THD\ Phase\ Terminal\ Voltage}{Intial\ THD\ Phase\ Terminal\ Voltage} + c_3 \times \frac{Intial\ Efficiency}{Efficiency} \quad (6)$$

3.4 Verifying using Finite Element Analysis

One of the significant characteristics of this proposed optimization method is the extremely close agreement between the values obtained from the optimization algorithm and the results from the FEA. To validate this claim, the results from FEA and the algorithm are compared in Table 5. The presented results provide evidence supporting the accuracy of the proposed optimization method.

Table 5. The comparison between the costs of the initial and final designs.

Parameters	Optimized Final Design	Initial Design
Weight Rotor Lam	449.6	475.7 Kg
Weight Damper Cage	24.26	0
Total Costs	3,317.02	3,329.9

4 Performance Assessment

In this section, the optimized generator is compared with the initial design (without a damper) under the same load and conditions, using the optimized variable values obtained from the previous section. The overall geometry and 3D shape of the optimized rotor, along with the flux density distribution, are shown in Fig. 9. The overall comparison results of the two designs are presented in Table 6.

Table 6. The overall comparison results of the two designs: initial and optimal

Optimization Objective	Unit	Value		
		Algorithm	Optimized Final Design	Initial Design
System Efficiency	%	95.56	95.53	95.9
|Output Power|	Kw	199.54	199.78	210.51
THD Phase Terminal Voltage	%	4.76	4.72	14.14

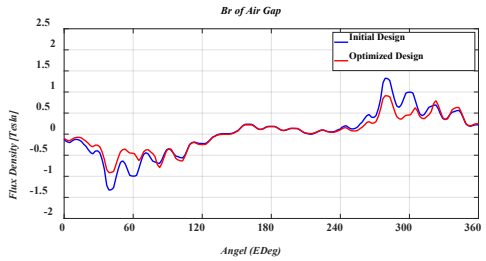

(a)

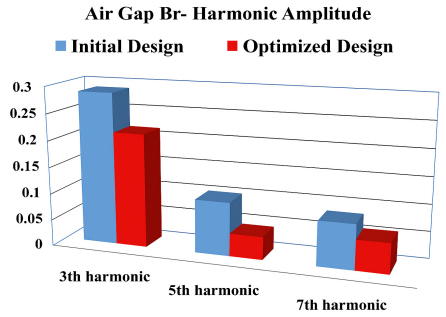

(b)

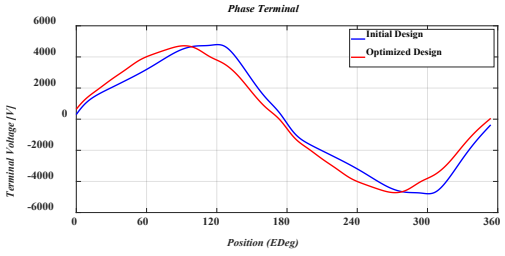

(c)

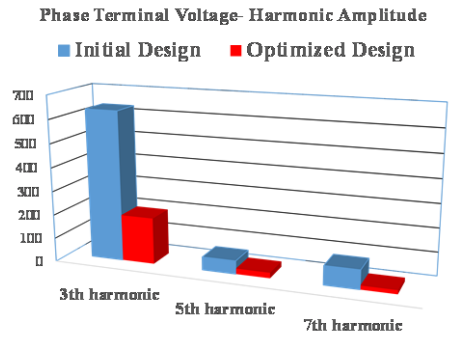

(d)

Fig 9. The radial flux density in the air gap and the terminal voltage output of the generator along with an analysis of its odd harmonics.

4.1 Terminal Voltage Harmonics

As mentioned, the output voltage harmonics have a very detrimental impact on the power system and generator. Magnetic harmonics that occur in the air gap of the generator are caused by the deviation of the ideal sinusoidal magnetic flux in the air gap. This deviation is due to mechanical design, non-uniform air gap, and the presence of current harmonics, and harmonics with frequencies that are multiples of the fundamental frequency (odd harmonics such as the third, fifth, and seventh harmonics) appear in it. The generator output voltage is produced based on Faraday's law from the changes in magnetic flux. Therefore, a new scenario has been adopted to reduce voltage harmonics, in which by optimizing the dimensions of the rotor bar, undesired harmonics in the radial flux density spectrum in the air gap are reduced, and consequently, the output voltage harmonics are also reduced. Fig. 10 shows the radial flux density in the air gap and the terminal voltage output of the generator along with an analysis of its odd harmonics. According to Fig. 10, it can be concluded that the adopted scenario was true, and by properly optimizing the geometric structure of the rotor without manipulating the stator structure and excitation, air gap harmonics have been reduced, and consequently, voltage harmonics have also been significantly reduced. As claimed, reducing the generated harmonics has also improved the mechanical behavior of the generator. The maximum stress on the rotor lamination in the optimized state is 28.78 megapascals, whereas in the initial design, this value was 34.27 megapascals. This indicates an increase in the safety and reliability of the improved generator [14], [15], [16].

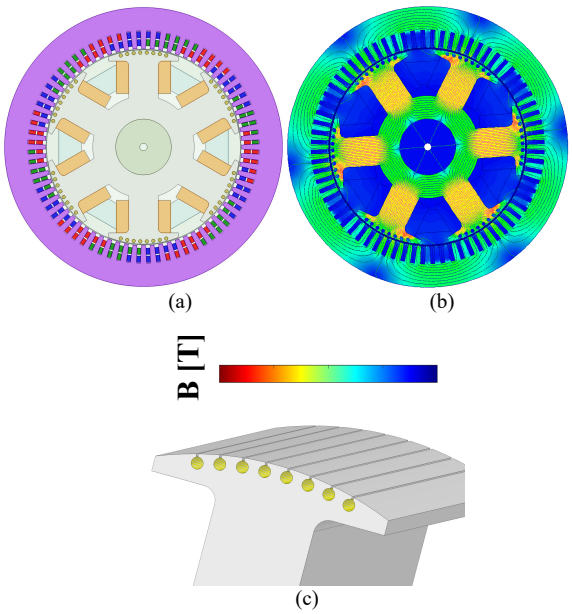

Fig 10. The overall (a) geometry and (b) flux density distribution, along with the (c) 3D shape of the optimized rotor.

4.2 Efficiency and Output Power

To calculate efficiency, all core and winding losses were determined. The stabilized value, along with an output power of 200 kW as indicated in Table 6, suggests low losses and satisfactory output power.

4.3 Analysis of Cost Changes and Usage of Brass (70% Cu, 30% Zn)

One of the critical factors in constructing power generators is cost. This section compares the cost variations between the optimal and initial designs. Before this comparison, it's important to note that the material of the dampers is crucial. Therefore, factors such as cost, weight, and appropriate output were considered when selecting the material. In this study, pure copper and brass (70% Cu, 30% Zn) were considered. By comparing the output of dampers made of copper and brass, it was observed that efficiency, power, and voltage harmonics differed very slightly. Therefore, for comparison, cost and weight must be considered. According to references [19], [20], the price per kilogram of copper is \$9.6 and the price per kilogram of brass (70% Cu, 30% Zn) is \$7. The weight of the damper cage under copper is 25.04 kg, and under brass, it is 24.26 kg. Therefore, the total cost of brass is less than pure copper. Finally, Table VI compares the costs of the initial and final designs. In this comparison, the price per kilogram of M350-50A is \$7, according to[20]. This comparison shows that the improved design, despite the addition of dampers, has also improved in terms of cost.

4.4 Mechanical Anslysis

Mechanical analysis is essential for optimal performance and preventing failures in WRSG systems. One of the challenges of adding a damper to the WRSG structure is the increased stress applied to the rotor lamination. Therefore, this paper aims to control these stresses by employing an appropriate optimization method and selecting suitable optimization variables. Due to the presence of non-idealities and oscillations in the electric machine's output torque (T_{out}), the resulting forces can be determined by solving the system's governing dynamic equations. These forces primarily appear in two forms: shear stress and axial stress. Given that T_{out} is directly transmitted by the rotor, the rotating component of the electric machine, all stress analyses focus on the rotor. In the nonlinear (plastic) region, beyond the yield point, the induced stress is typically defined as the applied force per unit area, as represented in Eq. 7.

$$\tau = F/A \tag{7}$$

where F represents the applied force, A denotes the contact area, and τ signifies the resulting stress. As illustrated in Eq. 8, the force is directly influenced by the rotor's angular velocity and mass, as well as the

eccentricity percentage. Consequently, as the angular velocity increases, the average stress value exhibits an exponential growth trend.

$$F = me\omega^2 \quad (8)$$

Here, m represents the mass, e denotes the eccentricity percentage, and ω is the rotor's angular velocity. Due to manufacturing uncertainties in electric machines, a certain degree of eccentricity is always present in the rotor. As a result, the forces, stresses, and vibrations of the machine can be analyzed under normal operating conditions. Beyond the nonlinear stress region, in the linear region, stress can be expressed as the ratio of the applied force to the corresponding area, as defined in Eq. 7. Alternatively, the yield stress can be formulated in Eq. 9 based on its dependence on Young's modulus of two designs and the applied tension. Consequently, different values of Young's modulus result in varying yield stresses.

$$\sigma = E\varepsilon \quad (9)$$

where, E is Young's modulus, ε is tension, and σ is yield stress. Incorporating a damper into the WRSG system was initially expected to increase the mechanical stress exerted on the rotor. However, through precise optimization and the careful selection of key parameters and methodologies, not only was the maximum stress prevented from rising, but it was effectively reduced, as shown in Fig. 11. This outcome highlights the significance of an optimized design approach in mitigating mechanical stress while maintaining system stability and performance.

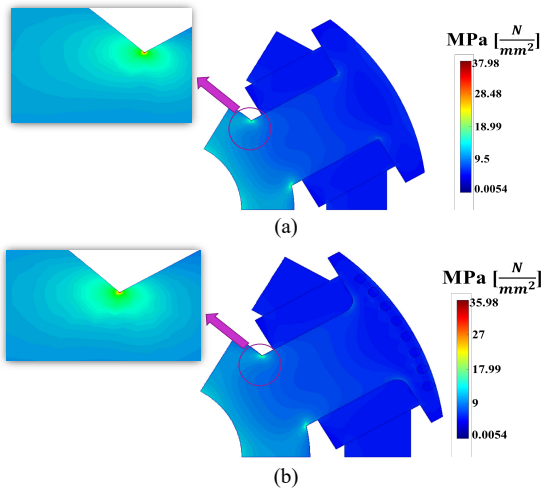

Fig 11. Von mises stress of the rotor (a) initial (b) optimized.

It is observed that the inclusion of damper bars does not lead to an increase in the von Mises stresses of the rotor. This outcome can be explained by the fact that the dominant contributor to the mechanical stresses is the centrifugal force generated by the rotor body and field winding mass. The damper bars, in contrast, constitute only a small portion of the total rotor mass and are mechanically embedded into the pole body or rotor slots, where they remain well supported. Their orientation is largely aligned with the direction of the principal stresses, which minimizes the introduction of additional stress concentrations. Consequently, while the damper bars strongly influence the electromagnetic and dynamic behavior of the machine, their contribution to the static mechanical stress state of the rotor is negligible, resulting in no significant change in the von Mises stress distribution.

4.5 Thermal Analysis

Thermal analysis of electrical machines can be carried out using various methods, with the most common being the Lumped Parameter Model (LPM), Finite Element Analysis (FEA), and Computational Fluid Dynamics (CFD). Each of these techniques has its own strengths and limitations. CFD offers detailed modeling of fluid flow and heat transfer, making it highly accurate for studying complex cooling mechanisms, but it requires significant computational resources and time. FEA provides high spatial resolution for analysing temperature distribution across components and is especially effective for validating thermal gradients and hot spots, although it also tends to be computationally intensive [21], [22]. In contrast, the LPM is a low-order thermal network model that simplifies the machine into interconnected thermal resistances and capacitances, offering much faster simulation times while still capturing the dominant heat transfer paths. This makes LPM especially suitable for early design stages, iterative optimization, and system-level studies where computational efficiency is critical [23].

In this study, both LPM and FEA were used to evaluate the thermal behavior of the WRSG under nominal load and steady-state conditions. The LPM approach modeled major components, such as stator windings, stator and rotor cores, shaft, and air gap, as thermal nodes connected through conduction and convection paths. Key heat sources included copper losses in the windings, iron losses in the magnetic core, and eddy current losses in the damper. Each node's temperature was determined using corresponding thermal resistances, capacitances, and power losses. To ensure accuracy, a steady-state thermal FEA simulation was also conducted, offering a more detailed spatial temperature distribution across machine components. The results of both methods were compared, and good agreement was observed between the LPM and FEA outcomes, validating the reliability of the simplified model.

The results indicate that the modified design illustrated a temperature reduction in key areas: stator winding average (from 87.3 °C to 78.5 °C), stator winding

hotspot (from 108.6 °C to 105.5 °C), field winding hotspot (from 119.6 °C to 116.0 °C), and rotor pole (from 100.3 °C to 97.0 °C). The detailed temperature distributions are shown in Fig. 12 (LPM) and Fig. 13 (FEA).

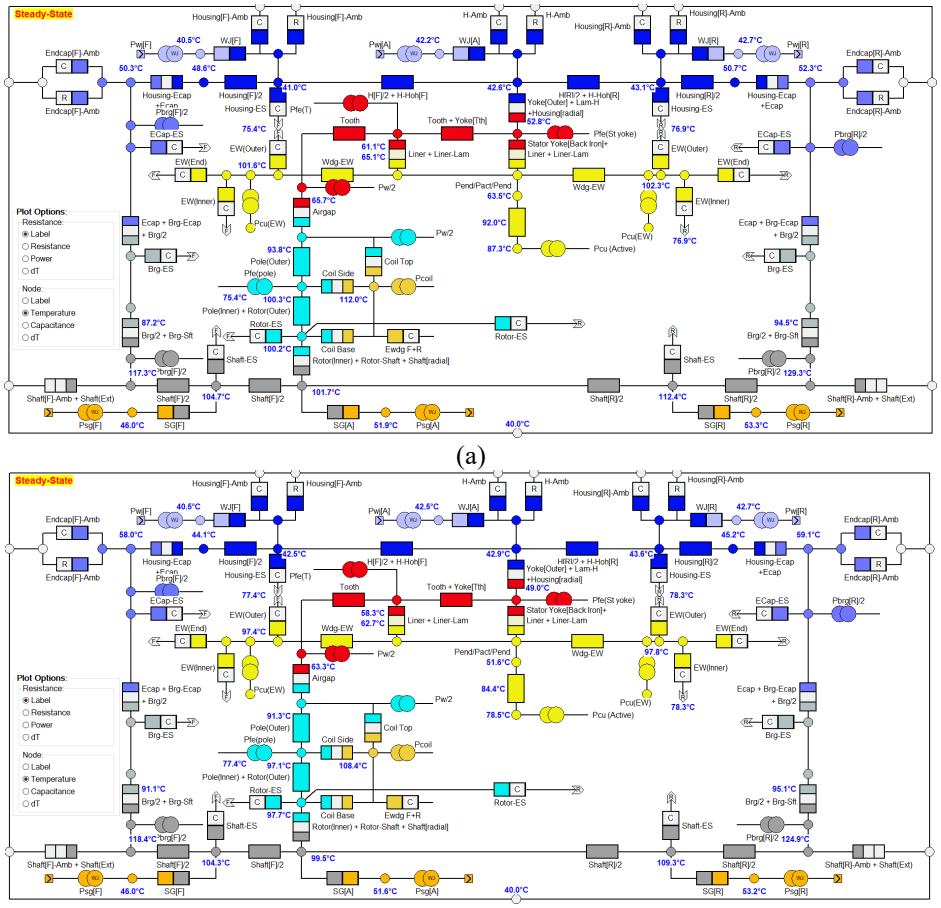

(a)

(b)

Fig 12. The LPM temperature analysis of the WRSG (a) initial (b) optimized.

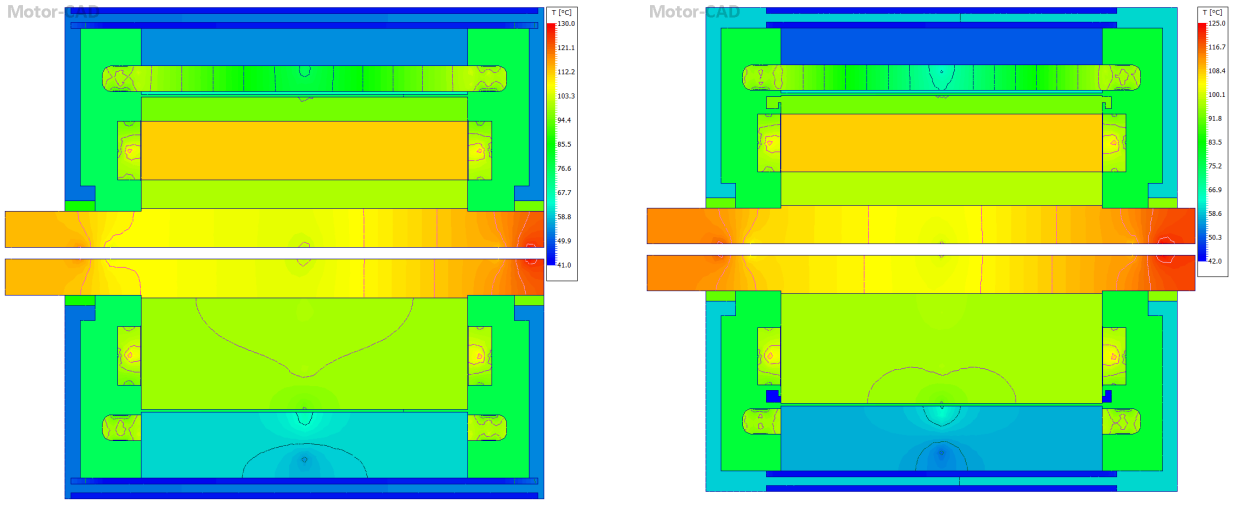

(a) (b)

Fig 13. The FEM temperature analysis of the WRSG (a) initial (b) optimized.

5 Future Works

Future studies will focus on extending the present analysis in two main directions. First, the influence of damper bars on transient torque during fault conditions, particularly under short-circuit scenarios, will be investigated to better understand their role in mitigating electromechanical stresses and enhancing rotor stability. Second, additional parametric studies considering variations in damper bar geometry and configurations will be carried out to evaluate their impact on both mechanical stress distribution and electromagnetic performance. Together, these efforts will provide a more comprehensive understanding of damper bar design trade-offs in electrically excited synchronous generators.

6 Conclusion

In this study, a WRSG was proposed for use in a power system that satisfies mechanical constraints. To achieve a voltage with lower harmonics, dampers were added. However, it is noted that incorporating classical dampers typically leads to significant efficiency and power losses. The damper proposed in this work, which includes notches between the damper and the air gap, optimized the structure and overcame these drawbacks. During the multi-objective optimization stage, a correlation analysis highlighted the significant influence of the damper's shape and dimensions. Using surrogate modeling, combined with efficient time and accuracy based on MNE and R^2 criteria, along with the PSO algorithm, the final design was determined. The mechanical analysis showed that the proposed damper design effectively minimized the maximum stress applied to the rotor lamination, thereby improving the generator's structural reliability. Thermal analysis, considering both steady-state and overload conditions, confirmed that the temperature rise under both normal and transient loads remained within safe limits. This comprehensive approach verified the performance, thermal stability, and structural integrity of the WRSG. Furthermore, an investigation into the damper materials revealed that brass, while lighter and cheaper than copper, provided performance comparable to the initial design without a damper, with no significant difference in generator efficiency, power output, or harmonic reduction.

7 References

[1] A. Amini, F. Mahmouditabar, N. J. Baker, and A. Vahedi, "Voltage Harmonics Reduction in WRSGs: A Multi-Objective Approach Using Surrogate Modeling with Enhanced Damping," *2024 4th International Conference on Electrical Machines and Drives (ICEMD)*, pp. 1–6, Dec. 2024, doi: 10.1109/ICEMD64575.2024.10963449.

[2] G. P. Hammond, "Energy, environment and sustainable development: A UK perspective," *Process Safety and Environmental Protection*, vol. 78, no. 4, 2000, doi: 10.1205/095758200530826.

[3] N. Abas, A. Kalair, and N. Khan, "Review of fossil fuels and future energy technologies," *Futures*, vol. 69, 2015, doi: 10.1016/j.futures.2015.03.003.

[4] R. Takarli *et al.*, "A Comprehensive Review on Flywheel Energy Storage Systems: Survey on Electrical Machines, Power Electronics Converters, and Control Systems," 2023. doi: 10.1109/ACCESS.2023.3301148.

[5] A. Amini, M. S. Khajueezadeh, and A. Vahedi, "Reliability and Lifetime Analysis on Permanent Magnet Motors in Elevator: Case Study PMA-SynRM & IPMSM," in *2023 3rd International Conference on Electrical Machines and Drives, ICEMD 2023*, 2023. doi: 10.1109/ICEMD60816.2023.10429474.

[6] F. Mahmouditabar, A. Vahedi, and F. Marignetti, "The Demagnetization Phenomenon in PM Machines: Principles, Modeling, and Design Considerations," *IEEE Access*, vol. 11, pp. 47750–47773, 2023, doi: 10.1109/ACCESS.2023.3274701.

[7] W. Fan and Y. Liao, "Impacts of flickers, harmonics and faults on synchronous generator operations," in *Proceedings of the Annual Southeastern Symposium on System Theory*, 2012. doi: 10.1109/SSST.2012.6195136.

[8] J. Q. Wang, P. C. Song, C. H. Cui, J. K. Li, and T. Yang, "Analysis of operation of synchronous generator under the distortion of harmonic current," in *Asia-Pacific Power and Energy Engineering Conference, APPEEC*, 2012. doi: 10.1109/APPEEC.2012.6307699.

[9] T. M. Blooming and D. J. Carnovale, "Application of IEEE STD 519-1992 harmonic limits," in *IEEE Conference Record of Annual Pulp and Paper Industry Technical Conference*, 2006. doi: 10.1109/papcon.2006.1673767.

[10] D. Fallows, S. Nuzzo, A. Costabeber, and M. Galea, "Harmonic reduction methods for electrical generation: A review," 2018. doi: 10.1049/iet-gtd.2018.0008.

[11] G. Traxler-Samek, R. Zickermann, and A. Schwery, "Cooling airflow, losses, and temperatures in large air-cooled synchronous machines," *IEEE Transactions on Industrial Electronics*, vol. 57, no. 1, 2010, doi: 10.1109/TIE.2009.2031191.

[12] S. Nuzzo, M. Galea, C. Gerada, D. Gerada, A. Mebarki, and N. L. Brown, "Damper cage loss reduction and no-load voltage thd improvements in salient-pole synchronous generators," in *IET Conference Publications*, 2016. doi: 10.1049/cp.2016.0203.

[13] S. Nuzzo, M. Degano, M. Galea, C. Gerada, D. Gerada, and N. Brown, "Improved Damper Cage Design for Salient-Pole Synchronous Generators," *IEEE Transactions on Industrial Electronics*, vol. 64, no. 3, 2017, doi: 10.1109/TIE.2016.2619321.

[14] A. Amini, M. S. Khajueezadeh, and A. Vahedi, "A Multi-objective and Multi level Optimization of IPMSM Case Study Dynamometer," in *2023 3rd International Conference on Electrical Machines and Drives, ICEMD 2023*, 2023. doi: 10.1109/ICEMD60816.2023.10429311.

[15] M. S. Khajueezadeh, M. Emadaleslami, F. Tootoonchian, A. Daniar, M. C. Gardner, and B. Akin, "Comprehensive Investigation of the Resolver's Eccentricity Effect on the Field-Oriented Control of PMSM," *IEEE Sens J*, vol. 23, no. 17, 2023, doi: 10.1109/JSEN.2023.3292896.

[16] F. Mahmouditabar, A. Vahedi, and N. Takorabet, "Robust Design of BLDC Motor Considering Driving Cycle," *IEEE Transactions on Transportation Electrification*, vol. 10, no. 1, pp. 1414–1424, Mar. 2024, doi: 10.1109/TTE.2023.3285650.

[17] A. Amini, H. Haghighat, and A. Vahedi, "Surrogate and Correlation- based Optimization of Out-Rotor PMSM: A Case Study on e-Bike with Enhanced Halbach Array," *2024 4th International Conference on Electrical Machines and Drives (ICEMD)*, pp. 1–7, Dec. 2024, doi: 10.1109/ICEMD64575.2024.10963588.

[18] F. Mahmouditabar, A. Vahedi, M. R. Mosavi, and M. H. B. Bafghi, "Sensitivity analysis and multiobjective design optimization of flux switching permanent magnet motor using MLP-ANN modeling and NSGA-II algorithm," *International*

Transactions on Electrical Energy Systems, vol. 30, no. 9, p. e12511, Sep. 2020, doi: 10.1002/2050-7038.12511.
[19] "The London Metal Exchange: https://www.lme.com/en/metals/non-ferrous/lme-copper."
[20] "alibaba: https://www.alibaba.com/product-detail/ ."
[21] R. Nasiri-Zarandi, A. Ghaheri, and K. Abbaszadeh, "Thermal Modeling and Analysis of a Novel Transverse Flux HAPM Generator for Small-Scale Wind Turbine Application," *IEEE Transactions on Energy Conversion*, vol. 35, no. 1, pp. 445–453, Mar. 2020, doi: 10.1109/TEC.2019.2936683.
[22] F. Mahmouditabar and N. J. Baker, "Design Optimization of Induction Motors with Different Stator Slot Rotor Bar Combinations Considering Drive Cycle," *Energies 2024, Vol. 17, Page 154*, vol. 17, no. 1, p. 154, Dec. 2023, doi: 10.3390/EN17010154.
[23] F. Mahmouditabar, A. Vahedi, and N. Takorabet, "Design and Analysis of Interior Permanent Magnet Motor for Electric Vehicle Application Considering Irreversible Demagnetization," *IEEE Trans Ind Appl*, vol. 58, no. 1, pp. 284–293, 2022, doi: 10.1109/TIA.2021.3126695.

ALI AMINI was born in Isfahan, Iran, in 1997. He received the B.Sc. degree in electrical engineering from the Faculty of Electrical Engineering, Yazd University, Yazd, Iran, in 2019 and he received the M.Sc. degree (Hons.) in electrical engineering with the Department of Electrical Engineering, Iran University of Science and Technology (IUST), Tehran, Iran, in 2022. His current research interests include wireless power transfer and performing finite element analysis (FEA), reliability analysis, multi-objective optimization, and the design of electrical machines.

FARSHID MAHMOUDITABAR received the B.Sc. degree in electrical engineering from Shahrekord University, Shahrekord, Iran, in 2016, and the M.Sc. and Ph.D. degrees in electrical engineering from the Iran University of Science and Technology, Tehran, Iran, in 2018 and 2021, respectively. From 2019 to 2021, he was an Electrical Machine and Powertrain Engineer with IKCO, where he designed and manufactured several water-cooled IM for EV applications. From 2021 to 2023, he was an Electrical Machine and Powertrain Engineer with MAPNA Locomotive company, where he designed and developed the electrical machines for diesel-electric and overhead-powered electric locomotives. In 2023, he joined Newcastle University as a Research Associate working on the design of electrical machines for manufacture. His main research interests include the design, modeling, and optimization of electrical machines.

NICK J. BAKER (Member, IEEE) received the M.Eng. degree in mechanical engineering from Birmingham University, Birmingham, U.K., in 1999, and the Ph.D. degree in electrical machine design for marine renewable energy devices from Durham University, Durham, U.K., in 2003. He was a Researcher of machine design with Durham University. He was with the Lancaster University's Renewable Energy Group, from 2005 to 2008. He has spent a period in the industry as a Senior Consultant of energy consultancy TNEI Services Ltd., Newcastle, U.K., from 2008 to 2010. He is currently with Newcastle University's Electrical Power Group. He is also a professor in emerging electric machines working on machines across the renewable, automotive, and aerospace sectors.

ABOLFAZL VAHEDI (Senior Member, IEEE) was born in Tehran, Iran, in 1966. He received the B.S. degree in electrical engineering from Ferdowsi University, Mashhad, Iran, in 1989, and the M.Sc. and Ph.D. degrees in electrical engineering from the National Polytechnic Institute of Lorraine, Nancy, France, in 1992 and 1996, respectively. He is currently a Professor with the Department of Electrical Engineering, Iran University of Science and Technology, Tehran, where he is the Head of the Special Machines and Drives Laboratory. His current research interests include the design, modeling, optimization, and fault detection of electric machines and drives.